NMR relaxivity of Ln^{3+}-based zeolite-type materials

G. A. Pereira,[a] D. Ananias,[ab] J. Rocha,*[b] V. S. Amaral,[c] R. N. Muller,[d] L. Vander Elst,[d] É. Tóth,[e] J. A. Peters*[f] and C. F. G. C. Geraldes*[b]

Received 22nd March 2005, Accepted 4th May 2005
First published as an Advance Article on the web 20th May 2005
DOI: 10.1039/b504082e

A series of zeolite-type silicates containing framework lanthanides and termed Ln-AV-9 have been synthesized. Fundamentally different from conventional zeolites, these materials have the composition $(Na_4K_2)(Ln_2Si_{16}O_{38})\cdot 10H_2O$ (Ln = Nd, Sm, Eu, Tb, Gd, Dy). ^{29}Si and ^{23}Na MAS NMR spectra of Sm-AV-9 indicate the presence of six and two distinct sites, respectively, in agreement with the crystal structure. Gd-AV9 exhibits a simple Curie paramagnetic behaviour with an effective magnetic moment of 7.97 μ_B, while Eu-AV-9 has a much lower magnetic susceptibility, with a very shallow temperature dependence. The ^1H longitudinal relaxivities of water (r_1), obtained for aqueous suspensions of several Ln-AV-9 materials with different Ln^{3+} ions, are very small (0.04–0.09 s^{-1} mM^{-1}) and almost independent of the Ln^{3+} ion, while their transverse relaxivities (r_2) are much larger (16–60 s^{-1} mM^{-1}) and proportional to μ_{eff}^4, where μ_{eff} is the magnetic moment of the lanthanide ion present. While r_1 of Gd-AV-9 suspensions is very small, the r_2 is substantial and proportional to B_0^2. The dependence of r_2 on μ_{eff}^4 and B_0^2 has been fitted using the model of outer-sphere diffusion of water around the particles in the long-echo limit. The results indicate that aqueous suspensions of Ln-AV-9, although inefficient in longitudinal relaxation, are very effective in enhancing transverse relaxation, particularly at high magnetic fields. They are, therefore, attractive as T_2 MRI contrast agents.

Introduction

The development of magnetic resonance imaging (MRI) techniques for medical diagnosis has been accompanied by research on water-soluble paramagnetic metal complexes as contrast agents (CAs).[1–3] Paramagnetic lanthanide chelates are extremely efficient as CAs, because they are very effective in increasing the proton relaxation rates ($1/T_1$ and $1/T_2$) of water. Their efficiency in enhancing relaxation rates is usually expressed in terms of longitudinal and transverse relaxivity, r_1 and r_2, defined as reciprocals of T_1 and T_2, respectively, and expressed in s^{-1} per mM of Ln. The relaxivity reflects the efficiency of the nuclear-electron dipolar coupling between the nuclear magnetic moment of the water protons and the electronic magnetic moment of the metal ion, which accelerates the proton relaxation in the surrounding water. The paramagnetic relaxation process is described on the basis of a model considering two distinct contributions: *inner-sphere*, related to the exchange rate between the bound water molecules and bulk water, and *outer-sphere*, related to water molecules diffusing near the paramagnetic centre during their translational diffusion,[2,3] MRI CAs are used to improve the contrast between normal and diseased tissues. MRI contrast agents must have low charge (osmolality), be highly stable (thermodynamic, kinetic), very soluble, non-toxic and tissue and cell specific.

The Gd^{3+} ion has attracted most attention due its large number of unpaired electrons ($4f^7$) and relatively long electronic relaxation times.[1] Commercially available MRI CAs for clinical use include $[Gd(DTPA)(H_2O)]^{2-}$ (DTPA = 3,6,9-tris(carboxy methyl)-3,6,9-triazaundecan-1,11-dioic acid) (Magnevist®, Schering AG, Berlin, Germany)[4] and $[Gd(DOTA)(H_2O)]^-$ (DOTA = 1,4,7,10-tetraazacyclododecane-1,4,7,10-tetraacetate) (Dotarem®, Guerbet, Aulnay-sous-Bois, France).[5] Once injected, these small hydrophilic molecules rapidly diffuse from the vasculature into the interstitial space without entering the cells, and are rapidly eliminated by the kidneys.[6] The fast development of MRI has generated an increased demand for organ-specific[7–9] and tissue-targeted CAs. Some examples of targeting groups are antibodies, receptor ligands and enzyme substrates.[10]

Magnetic particles have a wide range of applications as CAs,[11] as their pharmacokinetics depend on the particle size.[12] Intravenous administration is only possible for particle sizes below the μm, and larger particles can only be used for examination of the gastrointestinal tract. Several types of Gd^{3+} containing particles have been studied as potential CAs. Gd^{3+}-loaded nanoparticles of 120 nm diameter are potential CAs for the gastrointestinal tract and lymph nodes, since such particles are small enough to pass through the vasculature.[13] Fibrin-targeted paramagnetic nanoparticles were recently reported as

[a]*Department of Biochemistry, NMR Centre and Centre of Neurosciences and Cell Biology, University of Coimbra, Coimbra, Portugal. E-mail: geraldes@ci.uc.pt*
[b]*Department of Chemistry, CICECO, University of Aveiro, 3810-193 Aveiro, Portugal. E-mail: rocha@dq.ua.pt*
[c]*Department of Physics, CICECO, University of Aveiro, 3810-193 Aveiro, Portugal*
[d]*NMR Laboratory, Department of Organic Chemistry, University of Mons-Hainaut, Mons, Belgium*
[e]*Laboratoire de Chimie Inorganique et Bioinorganique, École Polytechnique Fédérale de Lausanne, Switzerland*
[f]*Laboratory of Applied Organic Chemistry and Catalysis, Delft University of Technology, Delft, The Netherlands*

CAs for diagnosis of human thrombus.[14] Gd^{3+}-loaded nano-sized ($d < 100$ nm) mesoporous silica particles have high r_1 and r_2 relaxivities, depending on the Gd^{3+} loading.[15]

Conventional zeolites doped with lanthanides have already been used as CAs. Gadolite is a Gd^{3+}-modified zeolite NaY for imaging of the gastrointestinal tract.[16–18] Zeolite NaY is a microporous aluminosilicate based on sodalite cages (truncated octahedra), the hexagonal faces of which are joined *via* O bridges. Eight sodalite cages outline a large cavity (or supercage) with a diameter of 12.5 Å. The diameter of the pore window of the supercages, which share a 12-membered ring, is 7.6 Å. The hydrated Ln^{3+} ions reside in the supercages, not in the zeolite framework. In aqueous suspensions of these materials, the relaxation enhancement may be described using a two-step mechanism. In the first step, the lanthanide ions and Gd^{3+} inner-sphere water molecules exchange with the water molecules in the zeolite cavities, while in the second step the latter exchange with the bulk water.[19] These suspensions have potential as T_1 contrast agents at low field and as T_2 agents at higher fields.[20]

The synthesis of a new class of stable microporous materials has recently been reported, consisting of mixed tetrahedral–octahedral framework silicates containing stoichiometric amounts of Ln^{3+} ions in the framework, rather than in the pores (Fig. 1).[21] These aluminium-free zeolite-type silicates (Ln-AV-9) are fundamentally different from conventional zeolites, have the composition $(Na_4K_2)(Ln_2Si_{16}O_{38})\cdot 10H_2O$ (Ln = Eu, Nd, Tb, Gd, Dy, Sm), and their structure consists of a siliceous double layer linked to a perforated octahedral layer made up of $Ln(O)_6$ octahedra and $NaO_4(H_2O)_2$ octahedra.[21] As Fig. 1 shows, the water molecules are not coordinated to the Ln^{3+} ions, a situation which is in contrast to the Ln^{3+}-loaded conventional zeolites. However, Ln1 is relatively close to water molecules in the open spaces of the perforated octahedral layers (see below). The K^+ ions and the water molecules reside within the large channels formed by the planar 8-membered silicate rings. These microporous Ln^{3+} silicates have pore sizes of over 4 Å and the crytallite size is in the range 5–10 μm. The Langmuir surface areas (measured from N_2 uptake) are *ca.* 100 m^2g^{-1}.

The structures and morphology of Eu-AV-9 and Tb-AV-9 have been characterised by a range of techniques, in particular electron microscopy (SEM, TEM), powder X-ray diffraction, thermogravimetric analysis and solid-state NMR.[21] Here we study the magnetic properties of Gd-AV-9, further analyse the structure of Sm-AV-9 by ^{29}Si, ^{23}Na and ^{17}O solid-state NMR, and evaluate the potential of Ln-AV-9 as CAs for MRI.

Experimental

The synthesis of the AV-9 was described by Ananias *et al.*[21] ^{23}Na and ^{29}Si MAS NMR spectra were recorded at 105.85 and 79.49 MHz, respectively, on an Avance (9.4 T, wide-bore) Bruker spectrometer. ^{29}Si MAS NMR spectra were recorded with 40° pulses, a spinning rate of 5.0 kHz and 60 s recycle delays. Chemical shifts are given in ppm from TMS. ^{23}Na MAS NMR spectra were measured using short and powerful radio frequency pulses (0.6 μs, equivalent to a 15° pulse angle), a spinning rate of 15 kHz and a recycle delay of 2 s. Chemical shifts are quoted in ppm from 1 M aqueous NaCl. The triple-quantum ^{23}Na MAS NMR spectrum of Sm-AV-9 was recorded using the *z*-filter three-pulse sequence. The lengths of the first and second hard pulses (radio frequency magnetic field amplitude υ_1 = 130 kHz) were 3.6 and 1.3 μs, respectively. The length of the third, soft, pulse (υ_1 = 10 kHz) was 12.5 μs. The MAS rate was υ_R = 15 kHz. 180 data points were acquired in the t_1 dimension in increments of 16.7 μs. The ppm scale of the sheared spectrum was referenced to υ_0 frequency in the υ_2 domain and to 3.78 υ_0 in the υ_1 domain (reference: 1 M aqueous NaCl). ^{17}O MAS NMR spectra were also recorded at 54.227 MHz on a Varian VXR-400 S spectrometer.

AV-9 suspensions were prepared by mixing the powdered solid with doubly distilled water containing 0.2% of xanthan gum as a surfactant and dispersing them in an ultrasonic bath for 5 min.[19]

^1H (300.155 MHz), ^{23}Na (79.353 MHz) and ^{17}O (40.670 MHz) NMR spectra in aqueous suspensions were recorded on a Varian INOVA-300 spectrometer. The ^{23}Na and ^{17}O chemical shifts were measured with respect to external 0.1 M NaCl in D_2O and D_2O respectively.

The longitudinal and transverse relaxation times, T_1 and T_2, were measured at 20, 60 (Mini-spec PC120 and PC160, respectively, spin analysers obtained from Bruker), 100 MHz and 200 MHz (on a Bruker Avance-200 console connected to a

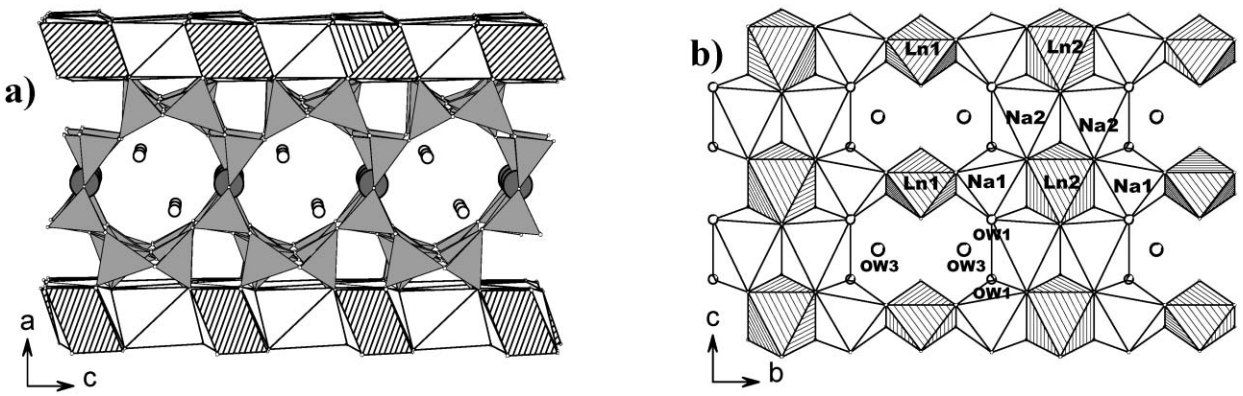

Fig. 1 Structure of Ln-AV-9 materials: (a) alternating octahedral sheet and double-silicate layer. The channels along the *b* axis are defined by 8-rings and are free from cations; (b) the octahedral layer, which has been cut away (does not represent a projection down the *a* axis).

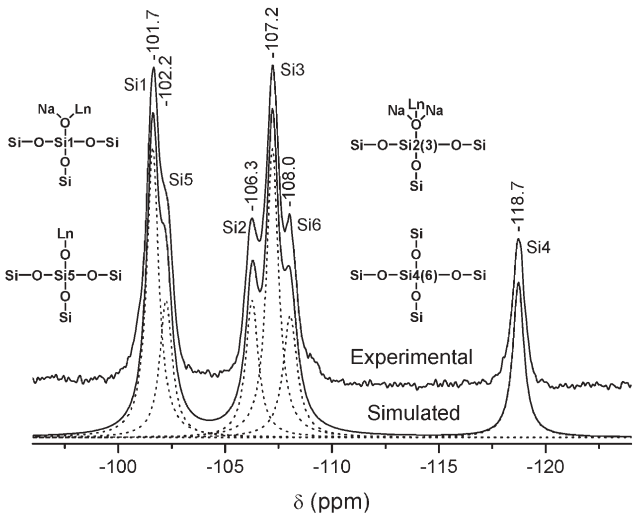

Fig. 2 Experimental, simulated ^{29}Si MAS NMR spectrum of Sm-AV-9 and local Si environments.

2.35 T (100 MHz) or 4.7 T (200 MHz) cryomagnet, 300 (Varian-INOVA spectrometer), 400 (Varian VXR-400 S spectrometer), 500 (Varian Unity 500 spectometer) and 600 MHz (Bruker AMX2-600 spectrometer), using an inversion recovery sequence for T_1 and a Carr–Purcell spin-echo sequence with two refocusing pulses of which the delay was varied for T_2. The values of T_2*, the transverse relaxation time in the presence local field inhomogeneities, were obtained from the water spectral linewidths. All experimental values of relaxation rates were corrected for diamagnetic contributions using suspensions of Y-AV-9 at the same concentration.

The computer fitting of the $1/T_2$ data was carried out with a homemade computer program using the Micromath Scientist version 2.0 (Salt Lake City, Utah, USA) software.

Magnetic susceptibility measurements were performed with a Quantum Design MPMS5 SQUID (superconducting quantum interference device) magnetometer. The measurements were taken under an applied magnetic field 100 Oe (7957 A m^{-1}) on heating from 5 K up to 300 K. The sample was previously cooled with the magnetic field applied from room temperature to 5 K.

Results and discussion

NMR structural characterization and magnetism

Because of the paramagnetism of the Ln^{3+} ions, good quality ^{29}Si MAS NMR spectra were only obtained for Sm-AV-9, as Sm^{3+} has the lowest magnetic moment. The spectrum in Fig. 2 displays six resonances at −101.7, −102.2, −106.3, −107.2, −108.0 and −118.7, in intensity ratios 2 : 1 : 1 : 2.1 : 1. This is in agreement with the crystal structure of AV-9 which calls for six distinct Si sites, two of which (Si1, Si3) with double population. The peak at −118.7 ppm is assigned to the Q^4 Si[4Si] environment Si4, because of the well-known correlation between the ^{29}Si isotropic chemical shift and the average Si–O bond distance (1.598 Å in Eu-AV-9) and Si–O–Si bond angle (154.0°).[22] The second Q^4 Si[4Si] Si6 environment gives the resonance at −108.0 ppm (average Si–O bond distance 1.623 Å and Si–O–Si bond angle 148.7°). Si2 and Si5 are Q^3 environments of the type Si[3Si; 1Ln, 2Na] and Si[3Si; 1Ln], respectively. Since the Si2 oxygen is linked to 1 Ln^{3+} and 2 Na^+ ions, it is charge deficient and the resonance at −106.3 is tentatively assigned to it. Thus, site Si5 resonates at −102.2 ppm. The peaks with double intensity at −107.2 and −101.7 ppm are attributed to Si3 and Si1, respectively.

The triple-quantum (3Q) ^{23}Na MAS NMR spectrum of Sm-AV-9 (Fig. 3) clearly shows the presence of two sites. Some residual intensity between the two peaks suggests that a third faint resonance may be present. Indeed, the simulation of the single-quantum spectrum requires the presence of a third (S3) peak, which we assume to be Gaussian in shape. Within the experimental error, the S1, S2, S3 populations are 1 : 1 : 0.2. The crystal structure AV-9 calls for two sites with 1 : 1 populations and S1 and S2 are attributed to these environments. S3 may be assigned to some Na^+ cations substituting for K^+ in the pores or to an amorphous material contaminating the sample (or to both). ^{23}Na NMR of AV-9 water suspensions revealed some sodium leaching (<2% of the total Na), possibly due the partial dissolution of the amorphous material present. Indeed, adding to these AV-9 suspensions the paramagnetic complex $[Tm(DOTP)]^{5-}$ shifts, the ^{23}Na NMR signal to higher frequency. Since $[Tm(DOTP)]^{5-}$ is too big to

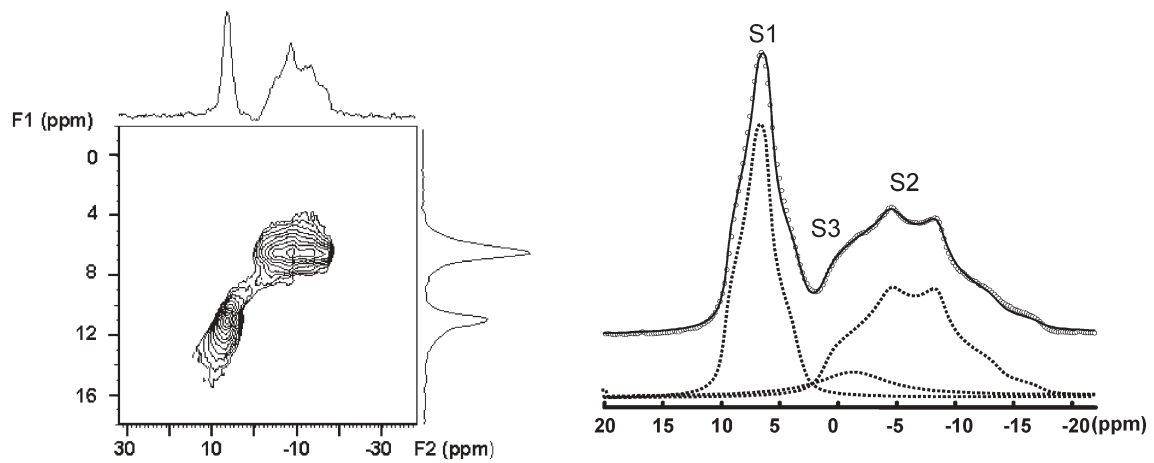

Fig. 3 Single-quantum (experimental and simulated) (right) and triple-quantum (left) ^{23}Na MAS NMR spectra of Sm-AV-9.

enter the AV-9 pores, the resonance is, thus, ascribed to a small amount of ^{23}Na in the water.

The simulation of the single-quantum spectrum yields the quadrupole coupling constant, C_Q, asymmetry parameter, η, and isotropic chemical shift, δ_{iso}, of S1 and S2, respectively: 1.05 and 1.80 MHz, 0.76 and 0.55, 9.5 and 1.7 ppm. Close examination of the O–Na–O bond angles and Na–O bond distances suggests that the local Na1 environment is more distorted than the Na2 one. Thus, peaks S1 and S2 are tentatively assigned to sites Na2 and Na1, respectively.

^{17}O MAS NMR spectra of Dy-AV-9 saturated with $H_2{}^{17}O$ (*ca.* 20% ^{17}O-labelling) contain a single unshifted resonance, with spinning sidebands (spectrum not shown), confirming that water molecules reside in the small zeolitic cavities. The ^{17}O resonance of water in conventional zeolites, such as LnNaY with big cavities, usually show no spinning side bands envelope in MAS spectra, even in the presence of paramagnetic ions.[23] The presence of spinning sidebands suggests that the diffusion of the water molecules is not too fast because they are present in small cavities. The high resolution ^{1}H and ^{17}O NMR spectra of Sm-AV-9 water suspensions, measured without spinning, show sharp resonances at 4.65 and 0 ppm, respectively. Since these signals exhibit almost no lanthanide-induced shifts the exchange between water inside and outside the material is slow on the NMR timescale and the ^{1}H and ^{17}O NMR signals of water inside AV-9 are too broad to be detected.

The magnetic susceptibility of Gd-AV-9 exhibits a simple paramagnetic behaviour following a Curie law with an effective magnetic moment of 7.97 μ_B, which compares well with the expected value for the $^8S_{7/2}$ Gd^{3+} ground state, 7.94 μ_B. This indicates that no magnetic coupling occurs between the Gd^{3+} ions in the zeolitic framework. The magnetic susceptibility of Eu-AV-9 is much lower, with a very shallow temperature dependence, reaching a constant plateau at low temperature ($T < 100$ K). This Van Vleck paramagnetic behavior[24] is characteristic of the $^7F_0$ Eu^{3+} ground state, which has no magnetic moment, and the temperature dependence arises only through the thermal occupation of states (mostly $^7F_1$).

Relaxometric studies

The influence of the concentration of the materials in aqueous suspension on the $1/T_1$, $1/T_2$ and $1/T_2$* values was studied for Dy-AV-9. The $1/T_1$ values obtained are proportional to the Dy-AV-9 concentration, giving a relaxivity value r_1 = 0.078 s^{-1} mM^{-1} ($\pm$0.015) at 300 MHz and 298 K.

The water ^{1}H r_1 and r_2 values were also obtained for aqueous suspensions of a series of Ln-AV-9 materials (Ln^{3+} = Nd^{3+}, Sm^{3+}, Eu^{3+}, Gd^{3+}, Tb^{3+}, Dy^{3+}). The longitudinal relaxivities at 300 MHz and 298 K (data not shown) are very small and almost independent of Ln^{3+} (*e.g.*, r_1 = 0.040 and 0.085 s^{-1} mM^{-1} for, respectively, Sm- and Tb-AV-9).

Platas-Iglesias *et al*[19] have studied GdNaY zeolite nanoparticles, considering a two-step water exchange model to explain the significant longitudinal relaxivities observed. The first step consists in the exchange between one of the seven water molecules coordinated in the inner-sphere of the Gd^{3+} ion bound to one oxygen atom of the zeolite framwork (Gd^{3+}-H distance of 3.1 Å) and the water molecules within the zeolite supercages (diameter 11.8 Å), followed by slow diffusion through the zeolite channels (diameter 7.4 Å) and exchange with the bulk water. This is not observed for Ln-AV-9 because: (i) Ln^{3+} ions are embedded in the framework as LnO_6 octahedra, water molecules have no access to the Ln^{3+} inner-sphere and are kept at large distances from it (3.9 Å in the small cavities of the octahedral layers, and 6.3 Å in the 4 Å diameter pores),[20] thus precluding the first step of the model; (ii) the water diffusion through the zeolitic channels is relatively slow; (iii) their exchange with the bulk water is also slow, as shown by ^{17}O and ^{1}H NMR. The small variation of r_1 with the effective magnetic moment may be ascribed to a dipolar effect.

On the other hand, the transverse relaxivities, r_2, of these Ln-AV-9 materials, obtained from linear plots of $1/T_2$ versus Ln-AV-9 concentration, are much larger than the corresponding r_1 values. The plot in Fig. 4 shows a linear dependence of r_2 on μ_{eff}^4, for the Ln-AV-9 (exception for Sm-AV-9) aqueous suspensions at 500 MHz and 298 K, where μ_{eff} is the effective magnetic moment of the lanthanide ions.[1]

The r_2 and r_2* relaxivities of Dy-AV-9 were compared at 300 MHz and 298 K, giving r_2 = 21.686 $s^{-1}mM^{-1}$ ($\pm$2.954) and r_2* = 405.947 $s^{-1}mM^{-1}$ ($\pm$51.876). The much larger values found for r_2* than for r_2 suggest the presence of high local field inhomogeneities and the loss of signal due to susceptibility differences, which may occur after only milliseconds.[25]

^{1}H relaxometric measurements were also performed as a function of B_0, in order to study the T_1 and T_2 effects as a function of the ^{1}H Larmor frequency. The longitudinal and transverse relaxivities of Gd-AV-9 (1.1 mg ml^{-1}; 1.28 mM of Gd^{3+} content, 298 K) are shown in Fig. 5.

The value of r_2 for Gd-AV-9 increases sharply with B_0^2 or the square of the ^{1}H Larmor frequency, $\omega_H^2 = \gamma_H^2 B_0^2$, where γ_H is the ^{1}H gyromagnetic ratio (see solid curve fitting). However, r_1 is almost field independent and much smaller than r_2. This behavior is typical of the Curie spin relaxation mechanism,[26] resulting from the modulation by the molecular motion of the

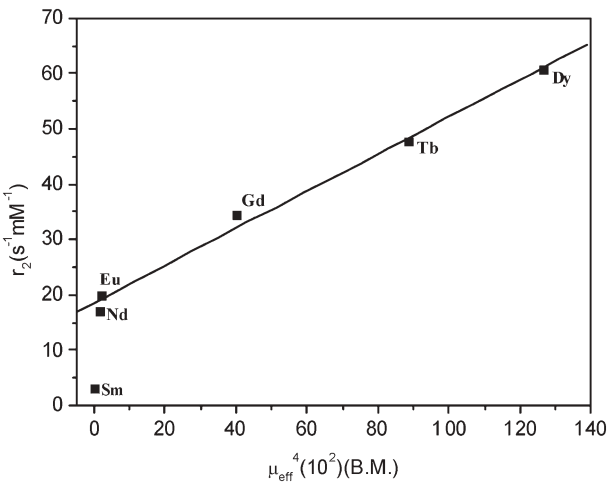

Fig. 4 Plot of water r_2 versus μ_{eff}^4 for the Ln-AV-9 aqueous suspensions at 500 MHz and 298 K.

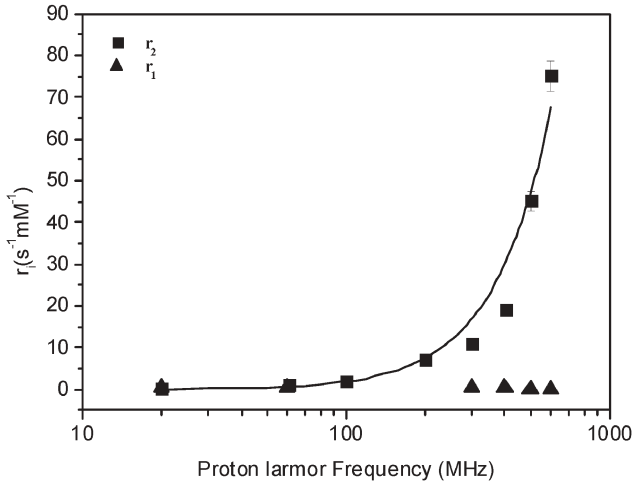

Fig. 5 Plot of experimental longitudinal (▲) and transverse (■) water relaxivity and calculated transverse water relaxivity (solid line) versus proton Larmor frequency at 298 K for Gd-AV-9 aqueous suspensions.

magnetic dipolar interaction between the water ^{1}H spins and the static magnetic moment of the paramagnetic centre, which results from the thermal average of its electronic spin levels. This can be applied to the weakly magnetized particles using the outer-sphere diffusion model,[27] under some limits. These limits depend on the relative magnitude of the following parameters: (i) τ_{CP}, defined as half the interval between successive 180° pulses in a CPMG sequence, (ii) τ_D, the time the water ^{1}H takes to diffuse to the surroundings of the magnetic ions or particles (no binding) and (iii) the time for a significant amount of dephasing to occur.[28]

The diffusion time is defined as $\tau_D = r^2/D$, where r is the effective radius of the spherical particle (or distance of closest approach) and D the diffusion coefficient. The relevant parameters in the outer-sphere (OS) theory, where the water ^{1}H diffuse past (without binding) the magnetic particles, are r, τ_D, $\Delta\omega_r$ (angular frequency shift at distance r) and v (volume fraction of magnetized particles). Assuming weakly magnetized particles ($\tau_{CP} < 1/\Delta\omega_r$), long-echo ($\tau_{CP} \gg \tau_D$) and high field limits, the OS contribution to $1/T_2$, in SI units, is:[29]

$$[1/T_2]_{OS} = (64\pi/135)1000N_A[M]\gamma^2(\mu_0\mu_C)^2\tau_D/r^3 \qquad (1)$$

where N_A is the Avogadro's number, μ_0 the magnetic permeability of vacuum, $[M]$ the molar concentration of the magnetized particles (in moles Ln^{3+}per liter) and μ_C their time-averaged magnetic moment. This equation may be rewritten as:

$$[1/T_2]_{OS} = (4/9)v(\Delta\omega_r)^2\tau_D \qquad (2)$$

where $v = 1000\ (4/3)\pi r^3 N_A[M]$, that is, the fractional volume occupied by the particles and $(\Delta\omega_r)^2 = (4/5)\ \gamma_H^2(\mu_0\ \mu_C)^2/r^6$, the mean squared frequency shift at the particle surface,[27] which is obtained by integrating the square of the z-component of the magnetic field, $B_z\ (r,\theta) = (\mu_C/r^3)(1 - 3\cos^2\theta)$, over a spherical surface of radius r and dividing by the surface area and the ^{1}H–^{1}H gyromagnetic radius, γ_H. The 'Curie moment'[26] is $\mu_C = -\mu_B\ g_J\ <S_z>$, where μ_B is the Bohr magneton, g_J the Landé g factor of the J manifold of the Ln^{3+} electronic ground state, with a spin expectation value $<S_z> = g_J\mu_B J(J + 1)B_0/3kT$, k being the Boltzmann constant.[30] The transverse relaxation rate predicted by the outer-sphere effect (eqn. 2) is proportional to μ_C^2 of the particles, through $(\Delta\omega_r)^2$, and thus to $\mu_{eff}^4 B_0^2$:

$$[1/T_2]_{OS} = C\mu_{eff}^4\gamma_H^2 B_0^2 \qquad (3)$$

where $C = (16/45)\mu_0^2 v\tau_D\mu_B^4/r^6(3kT)^2$, $\mu_{eff}^4 = g_J^4 J^2(J + 1)^2$ and $\gamma_H^2 B_0^2 = \omega_H^2$, which is the square of the ^{1}H Larmor frequency. Thus, the dependence of r_2 of Gd-AV-9 on ω_H^2 (Fig. 5) is explained by a Curie spin outer-sphere relaxation mechanism. The linear dependence of r_2 on μ_{eff}^4 observed for the Ln-AV-9 series (Fig. 4) also results from the predominance of this relaxation mechanism, although the large intercept (18.2 s^{-1} mM^{-1}) reflects the contribution of other mechanism(s), *e.g.*, a residual dipolar contribution from the Ln^{3+} ions closest to the water molecules diffusing next to the large (r *ca.* 3.5 μ), slowly diffusing (τ_D *ca.* 5.33 ms) particles.

Conclusions

Microporous paramagnetic silicates with stoichiometric amounts of Ln^{3+} ions in the framework, follow a simple Curie paramagnetic behaviour and are not efficient T_1 contrast agents. The r_1 of Gd-AV-9 suspensions is almost independent of the applied magnetic field. The enhancement of the longitudinal relaxation rate of water ^{1}H *via* the dipolar mechanism is low due to the relatively large distance between the water ^{1}H in the zeolite cavities and the framework Ln^{3+} ions. Furthermore, this small effect is not propagated to the bulk because the diffusion of water through the small zeolitic pores is slow. However, Ln-AV-9 (except Sm-AV-9) have large transverse relaxivities (r_2 = 16–60 s^{-1} mM^{-1}), proportional to μ_{eff}^4 of the Ln^{3+} and increase proportionally to B_0^2. The μ_{eff}^4 and B_0^2 dependence of r_2 was fitted using the model of outer-sphere diffusion of water around the particles in the long-echo limit. Thus, the particles containing Ln^{3+} ions with large μ_{eff} values (Gd^{3+}, Tb^{3+}, Dy^{3+}) are very effective T_2 MRI CAs, particularly at high magnetic fields. The r^{-4} dependence of r_2 of the particles on their effective radius (r) should also result in a dramatic r_2 increase with the decrease of particle size. As each particle contains a large number of Gd^{3+} ions per unit weight, these compounds may find applications in targeting CAs. A particular advantage of these materials is that they do not contain aluminium and the leaching of Ln^{3+} ions is difficult because they are part of the framework.

Acknowledgements

This work was performed within the framework of the EU COST Action D18 "Lanthanide chemistry for diagnosis and therapy" and the European-funded EMIL programme (LSHC-2004-503569). The work was supported by the Foundation of Science and Technology (F.C.T.), Portugal (project POCTI/QUI/47005/2002) and FEDER. É. Tóth acknowledges the Swiss National Science Foundation and the Swiss Federal Office for Education and Science for financial support.

References

1 J. A. Peters, J. Huskens and D. J. Raber, *Prog. Nucl. Magn. Reson. Spectrosc.*, 1996, **28**, 283.
2 P. Caravan, J. E. Thomas, T. J. McMurry and R. B. Lauffer, *Chem. Rev.*, 1999, **99**, 2293.
3 É. Tóth, L. Helm and A. E. Merbach, *Top. Curr. Chem.*, 2002, **221**, 61.
4 H. J. Weinmann, R. C. Brasch, W. R. Press and G. E. Wesbey, *Am. J. Roentgenol.*, 1984, **142**, 619.
5 J. P. Dubost, J. M. Leger, M. H. Langlois, D. Maeyer and M. Schaefer, *C. R. Acad. Sci., Ser. II*, 1991, **312**, 349.
6 R. C. Brasch, *Magn. Reson. Med.*, 1991, **22**, 282.
7 F. Cavagna, M. Daprà, F. Maggioni, C. de Haën and E. Felder, *Magn. Reson. Med.*, 1991, **22**, 329.
8 H. Schmitt-Willich, M. Brehm, C. L. J. Ewers, G. Mischl, A. Müller-Farnow, O. Petrov, J. Platzek, B. Radüchel and D. Sülzle, *Inorg. Chem.*, 1999, **38**, 1134.
9 R. B. Lauffer, D. J. Parmelee, H. S. Ouellet, R. P. Dolan, H. Sajiki, D. M. Scott, P. J. Bernard, E. M. Buchanan, K.-Y. Ong, Z. Tyeklar, K. S. Midelfort, T. J. McMurry and R. C. Walovich, *Acta Radiol.*, 1996, **3**, 5356.
10 (*a*) R. Weissleder, *Nat. Rev. Cancer*, 2002, **2**, 1; (*b*) L. Ciobanu, A. G. Webb and C. H. Pennington, *Prog. Nucl. Magn. Reson. Spectrosc.*, 2003, **42**, 69.
11 R. N. Muller, A. Roch, J.-M. Colet, A. Ouakssim and P. Gillis, in *The Chemistry of Contrast Agents in Medical Magnetic Resonance Imaging*, ed. A.E. Merbach and É. Tóth, John Wiley & Sons, Ltd., Chichester, 2001, p. 417.
12 R. Weissleder and P. Reimer, *Eur. Radiol.*, 1993, **3**, 198.
13 C. H. Reynolds, N. Annan, K. Beshah, J. H. Huber, S. H. Shaber, R. E. Lenkinski and J. A. Wortman, *J. Am. Chem. Soc.*, 2000, **122**, 8940.
14 X. Yu, S.-K. Song, J. Chen, M. J. Scott, R. J. Fuhrhop, C. S. Hall, P. J. Gaffney, S. A. Wickline and G. M. Lanza, *Magn. Reson. Med.*, 2000, **44**, 867.
15 Y.-S. Lin, Y. Hung, J.-K. Su, R. Lee, C. Chang, M.-L. Lin and C.-Y. Mou, *J. Phys Chem. B*, 2004, **108**, 15608.
16 K. J. Balkus, Jr., A. D. Sherry and S. W. Young, *U. S. Patent* 5122363 A, 1992.
17 I. Bresinska and K. J. Balkus, Jr., *J. Phys. Chem.*, 1994, **98**, 12989.
18 S. K. Sur, J. F. Heinsbergen and R. G. Bryant, *J. Magn. Reson., Ser. A*, 1993, **103**, 27.
19 C. P. Iglesias, L. V. Elst, W. Zhou, R. Muller, C. F. G. C. Geraldes, T. Maschmeyer and J. A. Peters, *Chem. Eur. J.*, 2002, **8**, 5121.
20 É. Csajbók, I. Bányai, L. Vander Elst, R. N. Muller, W. Zhou and J. A. Peters, *Chem. Eur. J.*, in press.
21 D. Ananias, A. Ferreira, J. Rocha, P. Ferreira, J. P. Rainho, C. Morais and L. D. Carlos, *J. Am. Chem. Soc.*, 2001, **123**, 5735.
22 G. Engelhardt and D. Michel, *High-Resolution Solid-State NMR of Silicates and Zeolites*, Wiley, Chichester, 1987.
23 Unpublished results.
24 J. H. Van Vleck, *Theory of Electric and Magnetic Susceptibilities*, Oxford, Oxford University Press, 1932.
25 J. Frahm, K. Merboldt, H. Bruhn, M. Gyngell, W. Hänicke and D. Chien, *Magn. Reson. Med.*, 1986, **3**, 321.
26 M. Gueron, *J. Magn. Reson.*, 1975, **19**, 58.
27 R. A. Brooks, F. Moiny and P. Gillis, *Magn. Reson. Med.*, 2001, **45**, 1014.
28 P. Gillis, A. Roch and R. A. Brooks, *J. Magn. Reson.*, 1999, **137**, 402.
29 Y. Gossuin, A. Roch, R. N. Muller and P. Gillis, *Magn. Reson. Med.*, 2000, **43**, 237.
30 I. Bertini and C. Luchinat, *Coord. Chem. Rev.*, 1996, **150**, 1.